IEEE Robotics and Automation Letters (RA-L) paper, presented at ICRA 2026, Vienna, Austria. Cite as RA-L paper.

Toward Simulation-Based Optimization of Compliant Fingers for High-Speed Connector Assembly

Richard Matthias Hartisch, Alexander Rother, Jörg Krüger, and Kevin Haninger

***Abstract*—Mechanical compliance is a key design parameter for dynamic contact-rich manipulation, affecting task success and safety robustness over contact geometry variation. Design of soft robotic structures, such as compliant fingers, requires choosing design parameters which affect geometry and stiffness, and therefore manipulation performance and robustness. Today, these parameters are chosen through either hardware iteration, which takes significant development time, or simplified models (e.g. planar), which can't address complex manipulation task objectives. Improvements in dynamic simulation, especially with contact and friction modeling, present a potential design tool for mechanical compliance. We propose and investigate feasibility of a simulation-based design tool for compliant mechanisms which allows design with respect to task-level objectives, such as success rate. This is applied to optimize design parameters of a structured compliant finger to reduce failure cases inside a tolerance window in insertion tasks. The improvement in robustness is then validated on a real robot using tasks from the benchmark NIST task board. The finger stiffness affects the tolerance window: optimized parameters can increase tolerable ranges by a factor of 2.29, with workpiece variation up to 8.6 mm being compensated. However, the trends remain task-specific. In some tasks, the highest stiffness yields the widest tolerable range, whereas in others the opposite is observed, motivating need for design tools which can consider application-specific geometry and dynamics. While the task simulation demonstrates a high accuracy for simple scenarios, achieving a 100% failure mode prediction, tasks with higher geometric complexity yield significant discrepancies between simulation and real-life, resulting in lower rates of 27.3% due to excessive simplifications of the simulated task. Failure during insertion can be modeled with a small sim2real gap, whereas failure during search and in-hand slip demonstrated a higher sim2real gap.**

***Index Terms*—Compliant joints and mechanisms, simulation and animation, grippers and other end-effectors.**

Received 11 September 2025; accepted 8 January 2026. Date of publication 19 January 2026; date of current version 27 January 2026. This article was recommended for publication by Associate Editor J. Bimbo and Editor J. Borras Sol upon evaluation of the reviewers' comments. This work was supported by European Union's Horizon 2020 Research and Innovation Programme under Grant 101058521. *(Corresponding author: Richard Matthias Hartisch.)*

Richard Matthias Hartisch and Alexander Rother are with the Department of Industrial Automation Technology, TU Berlin, 10587 Berlin, Germany (e-mail: r.hartisch@tu-berlin.de).

Jörg Krüger is with the Department of Industrial Automation Technology, TU Berlin, 10587 Berlin, Germany, and also with the Department of Automation, Fraunhofer IPK, 10587 Berlin, Germany.

Kevin Haninger is with the Department of Automation, Fraunhofer IPK, 10587 Berlin, Germany.

Digital Object Identifier 10.1109/LRA.2026.3655310

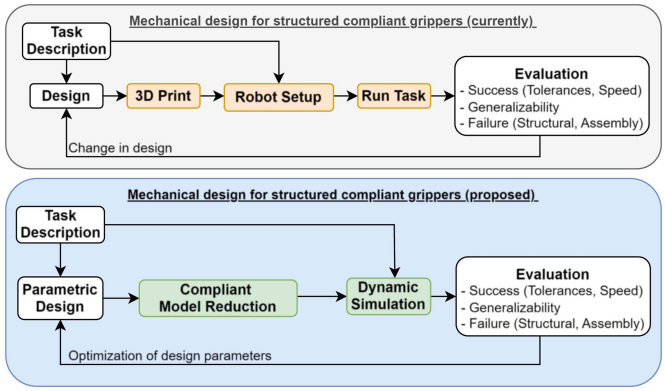

Fig. 1. Comparison of current (top) and proposed (bottom) design pipeline of passive, structured compliance. The objective is to reduce the need for real-life experiments, using instead a robot model and task (enter on the left) and dynamic simulation to evaluate a range of design and environmental parameters. The simulation results are evaluated according to robustness over part pose variation and failure cases. In this paper, these simulation results are compared against real execution.

I. Introduction

ROBUST contact-rich manipulation requires compensation for small errors in the contact geometry [1], [2]. Mechanical compliance offers compensation of variation in contact geometry through intrinsic dynamics; reducing the sensitivity to position variations and enabling self-correcting intrinsic dynamics, e.g. self-centering [3], [4]. The importance of compliance can be seen from its robotic applications: integrated in the kinematic structure [5], joints [6], flange [3], [7], fingers [1], [8], and environment [9], [10], [11]. Mechanical compliance directly affects normal forces and surface geometry during contact. This directly affects pressure distribution on contact areas, Coulomb friction limits, and the robustness uniformity over variation in object contact condition.

The mechanical design of compliance, however, is limited to lower-dimensional, simplified models (e.g. planar systems) to enable design analysis such as constraint-based design [12], effective TCP stiffness matrix [10], [13], or compliance ellipsoids [14]. While these methods can develop design intuition, they cannot scale to more complex designs. Topological optimization methods can improve the range of motion or linearity of compliant mechanisms [15], but has not been investigated for task-related performance. Mechanical parameters do not have the bandwidth limitations of active control [1], therefore methods for mechanical compliance design are considered here. As 3D printed compliant structures enables a larger design space,

IEEE Robotics and Automation Letters (RA-L) paper, presented at ICRA 2026, Vienna, Austria. Cite as RA-L paper.

methods are needed to optimize these designs with respect to task-level performance: e.g. robustness over part variation, in-hand slip, maximum collision force.

At the same time, dynamic simulation has substantially improved for robotics in terms of geometric complexity it can handle, numerical stability of simulation, differentiability, and realism. This offers a potential design tool for compliance, one which can scale in task and design complexity as well as provide task-level evaluation. Soft systems, e.g. compliant grippers, are numerically easier to simulate compared to stiff systems, which may allow for a reduced sim2real gap [16]. However, the question of simulation accuracy remains critical: is simulation accurate enough to motivate the design decisions in compliant device design? Simulation has been used as a tool to iteratively optimize fingertip contact geometry and grasping success [17], but not yet applied for compliant fingers.

To investigate applicability, MuJoCo is chosen as a physics-engine that focuses on contact-rich tasks with sufficient accuracy, modeling the 6- DOF stiffness between object contact and robot flange, and investigating if the simulation can predict the tolerance window in a resulting assembly task. Additionally, the ability to determine failure cases, i.e. slip, a failed search strategy and jamming of the plug is investigated. An overview of the approach can be seen in Fig. 1.

II. Task Description

This section describes the manipulation tasks considered, defining the assembly goal and failure cases.

A. Assembly Applications

Four assembly tasks have been chosen from the NIST task board, which are both simulated and carried out in real-life experiments. These include two rectangular shaped pegs in varying sizes (KET12 in Fig. 2(a) and KET8 in Fig. 2(b)), as well as two electrical connectors (RJ45 in Fig. 2(c) and USB in Fig. 2(d)). The assembly sequences utilized are similar for all assembly tasks and are further described in the simulation preparation in Section IV-B.

B. Robot Assembly Process

To achieve high-speed insertion, compliant fingers are used along with an assembly strategy, based on the search strategy employed in [1], which can can be seen in Fig. 3. First, the robot is positioned in its home position. Next, the robot is moved from the home position to above the connector within a safe distance. Next, it is lowered to the gripping height, after which the grippers are closed, grasping the part. The robot then moves upwards again to the previous position, while holding on to the connector. The aim of this process is to ensure that the connector is aligned with the socket before the assembly is performed via search strategy. The process is identical for all assembly tasks, except the starting position and the distance that the robot has to move for alignment are different.

The search strategy is performed following [1]: the connector is tilted by $5°$–$10°$, as seen in Fig. 3(a) and lowered to create line contact, visualized in Fig. 3(b). It is then moved in negative and positive x- direction (Fig. 3(c), 3(d)) to achieve planar contact, followed by a negative y- movement to establish a no-escape condition [18], shown in Fig. 3(e). A downward z- motion completes insertion (Fig. 3(f)).

(a) KET12 (b) KET8 (c) RJ45 (d) USB-A Connector

Fig. 2. The assembly tasks considered in this paper are shown.

C. Failure Cases

Practical design optimization for robotic tasks means reducing the incidence of failure cases, which we define next. Scenarios in which the connector is not properly assembled in the socket are defined as an unsuccessful assembly task.

During the assembly process, following, often interconnected, failure cases are possible and have been noted, which can be subdivided into four error sources: failure of the grippers, as demonstrated in Fig. 4, failed assembly due to the robot movement, occurring external forces and error sources from the plug and socket geometry and dynamics. The individual observed failures within the occurring assembly phases and the corresponding failure causes are listed in Table I in correspondence to the phase of assembly they are observed in. Failure case 1) depicts contact loss during grasping, manipulation and approaching, which has been noted by parameter combinations of low infill density and stiffness in combination with soft materials for PETG grippers [1]. Failure case 2) emphasizes on a failed search phase in which the plug is missed, as seen in Fig. 4(a), either due to a deficient search strategy movement and/or contact with the socket geometry. Both during the alignment and insertion the connector can be jammed, which is described in failure case 3) and visualized in Fig. 4(a). This occurs either due to insufficient stiffness in the assembly direction, occurring external forces from both dynamics and geometry of the connector, i.e. chamfers, which prevent centering of the connectors and therefore result in collision and jamming. Contact loss as failure case 4) is derived from insufficient normal- and friction force of the gripper and excessive external forces during contact between connector and socket, resulting in a loss of grip.

IEEE Robotics and Automation Letters (RA-L) paper, presented at ICRA 2026, Vienna, Austria. Cite as RA-L paper.

TABLE I
FAILURE CASES

Assembly Phase	Observed Problem	Failure Causes						
		Gripper			Movement	External Forces	Plug		Socket
		Normal Force	Friction Force	Insufficient Stiffness	Search Strategy		Dynamics	Geometry	Geometry
Grasping and Manipulation, Approaching	1) Contact loss	X	X	X					
Searching	2) Socket missed				X				X
Insertion	3) Connector jammed			X	X	X	X	X	
	4) Contact loss	X	X	X		X			

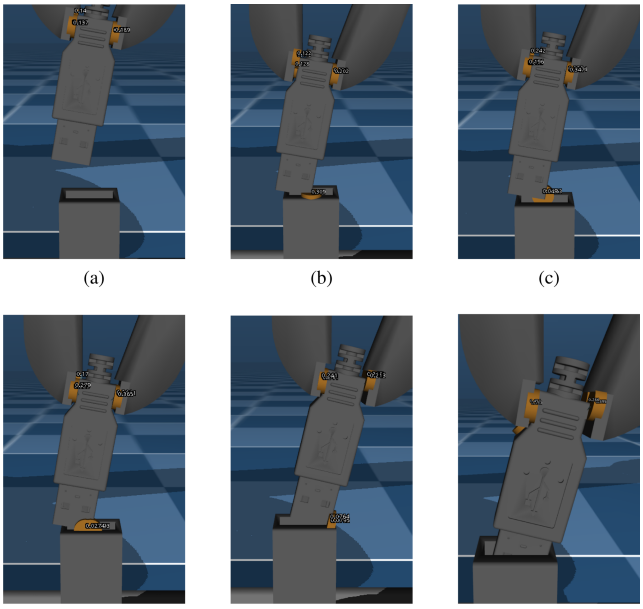

Fig. 3. Here, the simulated assembly movement is demonstrated exemplary for the USB assembly task. (a) and (b) visualize the approaching movement and first established contact on the socket. In (c) and (d) a back-and-forth motion of the connector in the x- direction with a slight movement in the z- direction is executed to allow the plug to slip into the socket when aligned. Following, in (e) contact is established between the sides of the plug and socket, realized by a motion in the negative y- direction. Insertion is completed with a downward z-direction motion as seen in (f).

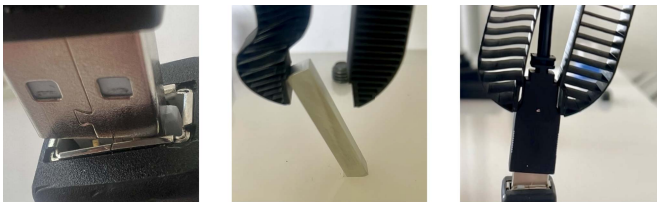

(a) Failure Case 2) - Socket missed

(b) Failure Case 3) - Connector jammed

(c) Failure Case 4) - Contact loss

Fig. 4. Visualized Failure Cases.

III. MODELING OF COMPLIANT FINGERS

The proposed design principle in [1] realizes a structured compliance through the internal structures of the fingers for passive alignment. Structured compliance allows the fingers to deflect under load, while providing sufficient stiffness, and therefore force, in the assembly direction, establishing contact only at the fingertip, as opposed to typical soft silicone- or finray-based soft grippers, which utilize an enveloping grip adapting to variation in surface geometry [19], [20], [21], [22], [23].

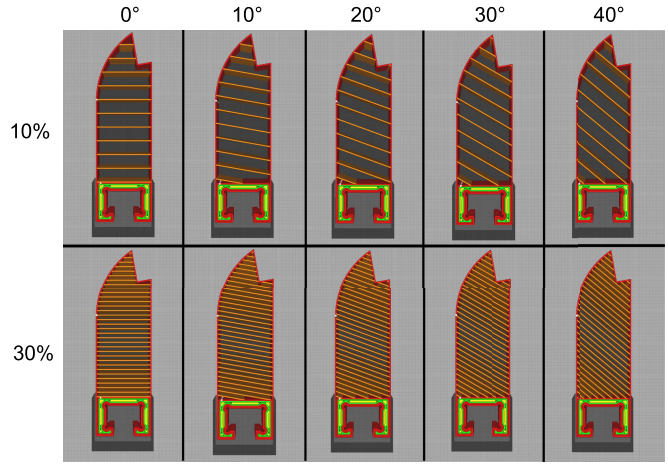

Fig. 5. Overview of varying infill parameters. Horizontally, the varying infill degrees between 0 ° and 40 ° are shown and vertically, the infill densities 10% and 30% are visualized. Generated in UltiMaker Cura.

A. Design Principle and Parameters

The identified design parameters in [1] are the infill options to adjust the density and orientation of the ribs in the finger, i.e. the infill direction (i), given in °, and the infill density (ii), given in %. The infill parameters can be seen in varying combinations in Fig. 5. This affects the bulk stiffness realized by the finger on a gripped part, as well as the maximum force that the finger can apply. Additionally, the compliant structure of the fingers enables an effective remote center of compliance (RCC), such that a lateral translation at the base of the plug causes a change in orientation, with the tip moving in the direction of the perturbation.

B. Stiffness Model

The stiffness model used in the simulation represents a simplified model of the finger, utilizing the stiffness values in the compliance direction [1]. As visualized in Fig. 3, contact is only established at the two contact planes in the fingertip. With the contact and stiffness resulting on the gripped part, sufficient search and assembly forces are provided. For this work it is therefore assumed, that each finger is modeled individually and the stiffness model of the compliant gripper can be sufficiently reduced to the physical contact between the notch of the fingers and the grasped parts utilizing only the diagonal entries of a 6-DOF stiffness matrix. While this is a significant simplification, 3- or 6- DOF models for RCC-effects are well-established [3]. This simplification was chosen for this work to enable simulation of dynamic, high-speed interaction, which requires computationally tractable dynamic simulation. FEA could capture continuous deformation, however, it is unsuitable for this scenario, as it is currently used for static analysis. Nonetheless, FEA can

IEEE Robotics and Automation Letters (RA-L) paper, presented at ICRA 2026, Vienna, Austria. Cite as RA-L paper.

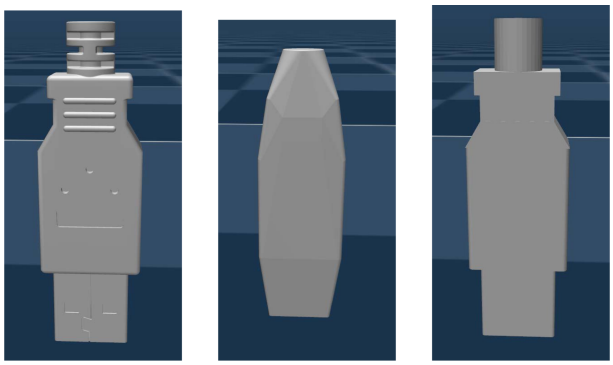

Fig. 6. Here, the different models used for simulation can be seen: (a) the original model to be simulated, (b) the convex auto-decomposition provided by MuJoCo, and (c) the manual remodeling in Blender.

be used to establish the simplified model parameters (stiffness values [1], location of RCC), allowing the effect of general design parameters such as infill direction to be considered in a more accurate way. This "compliant model reduction" can be seen in Fig. 1.

IV. Simulation Preparation

This section describes the geometric modeling of the connectors and simulation setup. The simulation and the used files are available at https://github.com/richardhartisch/mujoco_tasksim.

A. Convex Decomposition

MuJoCo can only handle convex meshes when performing peg-in-hole operations. Therefore, the connector and socket components, as well as the NIST Task Board itself, need to be decomposed. While MuJoCo offers an in-built option to auto-decompose structures into small convex parts, the approximation for complex structures like a connector, visualized in Fig. 6(a), is imprecise, leading to significant changes in tolerance, as seen in Fig. 6(b). Open-source solutions as [24] can be used to decompose the geometries beforehand, providing multiple options to adjust the quality of the decomposition. Alternatively, the model can be decomposed manually using simple convex structures, such as cubes and cylinders in Blender, as demonstrated in Fig. 6(c), ensuring a realistic approximation of the real part considering dimensions and tolerances.

B. Robot Movement

The assembly simulation uses two motion strategies: a tolerance-based and a duration-based method. Both step the model in a while-loop and update the viewer.

The tolerance-based method overwrites joint positions, moving the robot instantly and without actuator forces. It is used for the home pose and the preparatory phase until the TCP–target distance falls below $1 \cdot 10^{-3}$ m. During search, however, emerging contacts prevent reliable convergence, so the duration-based method is used instead, applying forces over a fixed time for all contact-rich motions.

After defining the poses, the search strategy (Section II-B) executes identically across tasks, differing only in initial pose and trajectory length. The tolerable range is obtained by shifting the initial search-start position in ± 0.1 mm increments until assembly fails. The maximal successful shift defines the tolerance range. Simulation and validation use MuJoCo's viewer and a Python script that loads the MJCF model with full parameter access. The MJCF implementation follows next.

C. Simulation Inputs

Models in MuJoCo are built by defining objects, properties, constraints and an environment through a MJCF. The complex mechanical properties of the structured compliant grippers can be modeled by six joints with specific stiffness values. Three slide joints are used for the translational movement and three hinge joints for the rotational movement, therefore defining the direct, diagonal stiffness values of a 6- DOF stiffness matrix, omitting the coupled, off-diagonal stiffness values in correspondance to the stiffness model in Section III-B. The three transversal slide joints are positioned in the center of the gripping surface. The placement is only relevant for visualization of the position of the TCP. The actual position of the slide joint has no impact on the gripper's movement as it can only move along the joint's axis. The position of the three hinge joints for the rotations about the x-, y- z- axis on the other hand is important as it influences the movement of the gripper and the applied forces due to the leverage. In accordance to the assumptions in [1], the center of rotation is positioned at the estimated RCC. Here a significant simplification from previously published work on the RCC position has to be noted. As described in [1], the position of the RCC depends on the infill parameters, i.e. the infill direction which influence the stiffness of the gripper. As only the stiffness values are given as an input, the varying position is not considered in this modeling, instead a fixed RCC position at $21\ mm$ in the z- direction from the contact plane is set. This represents a significant simplification, which is validated later in Section V-E. Joints in MuJoCo have an option to adjust their stiffness and damping values, for which the values obtained in [1] are utilized. As the stiffness values in x- direction and the rotations have not been determined in [1], assumptions are necessary. Considering the forces while gripping and the leverage, the stiffness is estimated between $0.5 - 2\ \frac{Nm}{rad}$. For the other joints, the stiffness was set to approximately 10 times the value of the hinge joint for the x- rotation's values. This was defined according to their real-life behavior, as they behave stiff on the real system. Thus, their impact in the simulation should be close to zero. Important contact parameters include the damping and friction between the connecting pairs gripper-connector and connector-socket. As the contact surface of the gripper has been equipped with a rubber layer the friction coefficient has been set to 1. As the contact between the connector and the socket typically represent smooth contact surfaces between metal and plastic, a low friction coefficient of 0.2 was chosen. The damping ratio was set to 1 to achieve a critical damping value between the connector and the gripper and an underdamped value of 0.5 for the contact between connector and socket.

V. Simulation and In-Situ Experiments

The simulation is performed for each NIST assembly task in MuJoCo and in-situ utilizing the aforementioned input values. The evaluation is carried out by observing the simulation process in the MuJoCo viewer. A successful assembly is defined as the full insertion of the connector inside the socket.

IEEE Robotics and Automation Letters (RA-L) paper, presented at ICRA 2026, Vienna, Austria. Cite as RA-L paper.

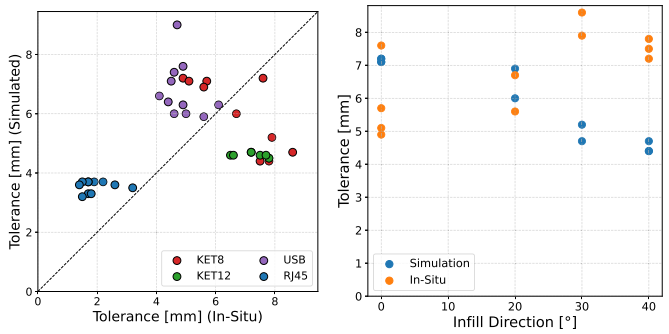

(a) (b)

Fig. 7. In (a) a comparison and conformity of simulated and in-situ tolerable ranges is given, in (b) the simulated (blue) and in-situ (orange) tolerable ranges across the Infill Direction for the KET8 assembly task are presented.

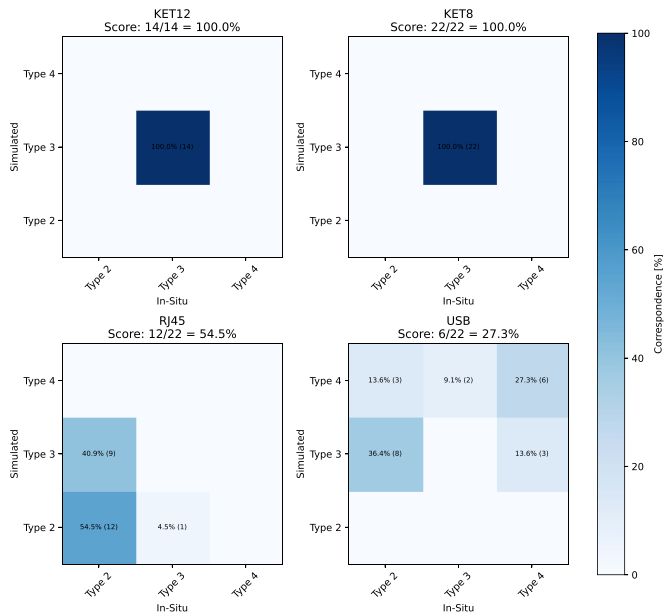

Fig. 8. In-Situ (x) and Simulated (y) failure cases observed during the assembly task.

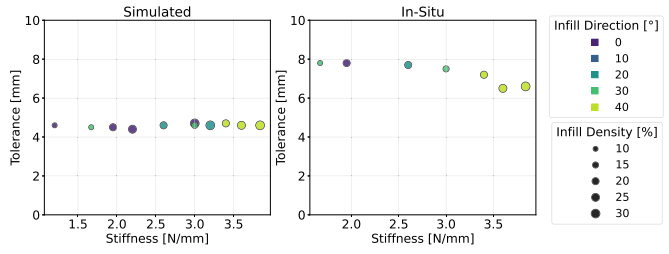

Fig. 9. Simulated (left) and In-Situ (right) tolerable ranges across design parameters for the KET12 assembly task.

A comparison and conformity of the simulated and in-situ tolerable ranges of the four assembly tasks is given in Fig. 7(a). In the Figs. 9, 10, 11 and 12, the observed tolerable ranges for each stiffness in the compliance direction is shown. The left diagram displays the simulated results and on the right side the corresponding in-situ results are visualized. The infill direction is indexed by five different colors and the increasing infill

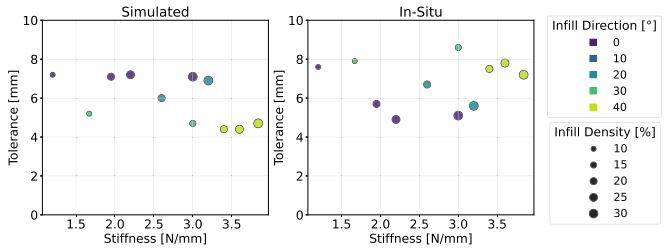

Fig. 10. Simulated (left) and In-Situ (right) tolerable ranges across design parameters for the KET8 assembly task.

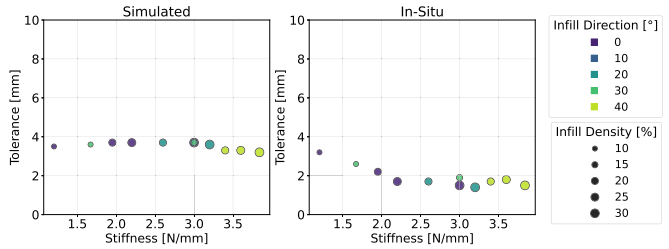

Fig. 11. Simulated (left) and In-Situ (right) tolerable ranges across design parameters for the RJ45 assembly task.

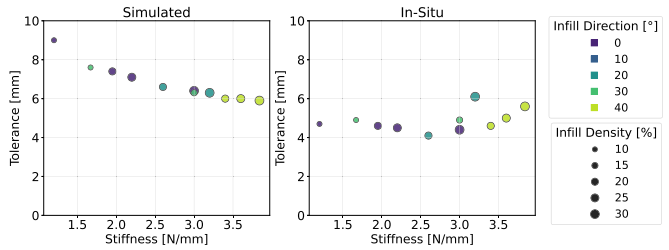

Fig. 12. Simulated (left) and In-Situ (right) tolerable ranges across design parameters for the USB assembly task.

density with an increasing size of the markers. Subsequently, the assembly tasks are evaluated in real-life, in-situ experiments.

In Fig. 8 heatmap visualizations are given of the observed failure cases. The x- axis depicts the failure types of the in-situ trials and the y- axis the observation from the simulated trials. For each evaluation the overall score is given.

Throughout all in-situ and simulated experiments, failure case 1) has not been detected. While in preliminary experiments in [1] in-finger-slip, i.e. failure case 1) has been noted for low-stiffness-grippers of PETG, these parameter combinations were not used in these experiments. The experiments are sorted in an increasing order according to their level of geometric complexity. As the KET components visualized in Fig. 2(a) and (b), consist of a rectangular-shaped peg assembled in a rectangular slot, these are ranked the lowest in terms of complexity. This is followed by the marginally more complex RJ45 task, as additional contact planes in both the plug and socket are introduced here, as seen in Fig. 2(c). The task with the highest complexity is the USB assembly task, which is visualized in Figs. 2(d), 4(a), and 4(c). Here, only few marginal contact planes are present on the connector. As illustrated in Figs. 2(d) and 4(a), the geometry of the plug adds an additional level of complexity due to the center bar inside the plug.

IEEE Robotics and Automation Letters (RA-L) paper, presented at ICRA 2026, Vienna, Austria. Cite as RA-L paper.

A. Evaluation of KET12

In the KET12 assembly task, the tolerable ranges remain relatively consistent regardless of any changes in the design parameters, as seen in Figs. 7(a) and 9. Optimized parameter combinations with low stiffness in the compliance direction of $1.67 - 1.95$ N/mm achieve the highest tolerable ranges in the in-situ trials in this task. The optimum increases the tolerable range by a factor of ≈ 1.2 (from 6.5 mm to 7.8 mm). The main observed failure type lies within the insertion, indicating an excessive inclination of the metal peg as the contributing factor, which results in jamming. Further, the simulated tolerable ranges are lower than in real-life, which achieve up to $\approx 74\%$ higher tolerable ranges. Jamming has consistently been observed throughout the trials.

B. Evaluation of KET8

The simulated tolerable ranges for KET8 are highest for low stiffness in compliance direction, of $\approx 7\ mm$, as visualized in Fig. 7(a) and Fig. 10. It is found, that the tolerable range decreases up to $2.5\ mm$ with an increasing infill direction. The in-situ experiments, however, achieve a higher range, as seen in Fig. 7(a) and Fig. 10. The parameter combinations with $0\circ$ infill direction achieve the highest range. As the scattering of the tolerable ranges of the KET8 assembly task has precluded a statement on an observable trend in Fig. 10, another approach is necessary. As seen in Fig. 7(b), a trend is observable on the tolerable ranges depending on the infill direction. With an increasing infill direction the tolerable ranges are reduced in the simulation, whereas the real-life validation demonstrates a higher tolerable range with an increased infill direction. It is therefore assumed, that the tolerable ranges of the KET8 task correspond to the effective RCC location influenced through the varying infill direction [1]. The significance of this effect in comparison to the general stiffness is attributed to the slender and long structure of the KET8 beam. It is therefore assumed, that for a correct representation of the real-life behavior for assembly tasks of objects with a high length-to-width ratio a more complex modeling in the simulation needs to be applied which enables the consideration of the varying RCC location.

The maximum shift in negative and positive direction is limited by connector jamming in both simulation and in-situ trials, as seen in Fig. 8, which is denoted by failure type 3). The plug is evaluated as a source for errors, as jamming has been observed due to a rotational movement about the y- axis of the connector when establishing contact with the back plane of the plug. This results in a rotational movement of the object, causing jamming and thus permanently damage of the grippers. Optimized parameter combinations with higher stiffness in the compliance direction of 3 N/mm achieved the highest tolerable ranges in the in-situ trials of this task. The most effective parameter set increased the tolerable range by a factor of ≈ 1.76 (from 4.9 mm to 8.6 mm).

C. Evaluation of RJ45

For the RJ45 assembly task the overall lowest tolerable range was observed both in the simulation and in-situ experiments as observed in Figs. 7(a) and 11. While the simulated values indicate consistent behavior over stiffness and infill parameter variation, the real-life experiments demonstrate an increasing tolerable range over decreasing infill density values in low-stiffness values of < 2.5 N/mm. Optimized parameter combinations with the lowest stiffness in the compliance direction of 1.2 N/mm achieved the highest tolerable ranges in the in-situ trials of this task. Optimal design parameters increased the tolerable range by a factor of ≈ 2.29 (from 1.4 mm to 3.2 mm). Failure cases 2) and 3) have been noted in the simulated trials, whereas failure case 2) was predominantly observed in the real-life validation, as seen in Fig. 8. In both cases the maximum shift was limited by the employed search strategy, which is attributable to the complex geometry of the RJ45 connecting pair. In these cases the connector collided with the outer geometry of the socket during search with an excessive shift in the positive direction causing the connector to miss the socket. This was observed through all trials in the simulated and in-situ experiments, possibly explaining the close similarity of the tolerable ranges and the consistency in the simulation. While failure case 3) was observed in the simulation, this was only noticed once during the in-situ trials, as a failed search strategy has been observed as the main failure case with one exception at the highest tolerable range. This results in a correspondence score of $54.5\ \%$ for the RJ45 assembly task.

D. Evaluation of USB

The simulated USB assembly task demonstrate a clear observable trend on the tolerable ranges in Figs. 7(a) and 12. A comparably large tolerance window of up to 9 mm could be achieved, the minimum tolerable range is specified with 5.9 mm for the combination with the highest stiffness. Especially in this trial the differences between simulation and real-life experiments become evident, as the results obtained from the in-situ experiments exhibit a virtually inverse tolerable range over the infill parameters where the highest tolerable range corresponds to the lowest achievable range in the simulated trial. Optimized parameter combinations with high stiffness in the compliance direction of 3.2 N/mm achieved the highest tolerable ranges in the in-situ trials of this task. Optimal design parameters increased the tolerable range by a factor of ≈ 1.49 (from 4.1 mm to 6.1 mm). Additionally, for this assembly scenario different failure types are observed. While jamming and contact loss is determined in the simulation, this does not correspond to the in-situ trials, which are not unambiguously attributable to a specific parameter combination, as summarized in Fig. 8. A clear correlation between the infill parameters and failure case seen in-situ is not visible. Therefore, the correspondence in this scenario is evaluated with only $\approx 27.3\%$. The following section discusses the assumptions for these deviations.

E. Sensitivity Study

Following the simulation results, a sensitivity analysis was conducted exemplary on the KET12 assembly to evaluate the influence of the contact parameters, i.e. the friction coefficient and damping ratio on the tolerable range. The resulting tolerances were scaled. Friction coefficients ranged from 0.2 (smooth plastic–metal) to 1.4 (rubber–concrete). For the damping ratio, under- (< 0), over- (> 0), and critically (0) damped cases were tested. As shown in Fig. 13, the predicted tolerance window does not change to moderate parameter variations within realistic bounds. For the gripper–connector contact, tolerable ranges stayed largely constant down to a friction coefficient of 0.2. Below this, grip loss and jamming reduced the tolerance to $\approx 39\%$, and further reduction caused complete assembly failure.

IEEE Robotics and Automation Letters (RA-L) paper, presented at ICRA 2026, Vienna, Austria. Cite as RA-L paper.

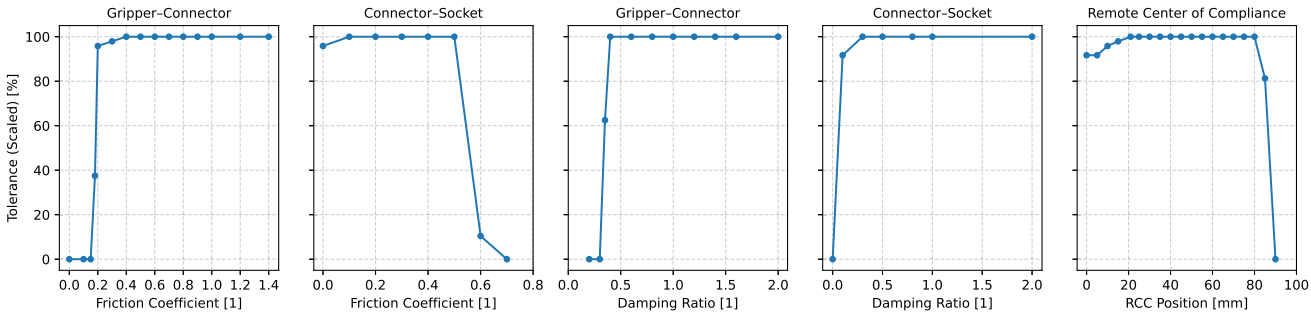

Fig. 13. Analysis on influence of parameter variation on the scaled tolerable range for KET12 assembly task including the friction coefficient and damping ratio between the gripper-connector contact and connector-socket contact and the position of the RCC in the z- direction.

Higher friction showed no adverse effects. For the connector–socket contact, increasing friction from 0.5 to 0.6 and 0.7 caused failure due to excessive resistance during the search motion. Reducing the stiffness to 0 produced initial instabilities, which the search strategy compensated, yielding a slightly reduced tolerance ($\approx 95\%$). For the connector–gripper contact, lowering the damping ratio to 0.35 reduced the tolerance to $\approx 60\%$, and 0.3 caused failure due to an insufficient grasping force. Overdamping (2.0) had no effect. Similar behavior was observed for the connector–socket interaction: minor deviations emerged at a damping ratio of 0.1, and a non-damped system (0) failed entirely, while overdamping had no influence. Overall, maintaining realistic friction and damping values demonstrates a low sensitivity of the simulation to contact parameter variations of approximately $\pm 20\%$. As described earlier, the infill parameters influence both the overall stiffness and the RCC position, which was kept fixed in this simulation. For a dynamic RCC model an adjustment would have to be included of the hinge joint positions, as well as an adjustment of the corresponding stiffness values, depending on the infill parameters. To assess this effect, a sensitivity analysis of the RCC position in the $z-$ direction was performed, examining its impact on the tolerable range. The results can be seen in Fig. 13. Shifting the RCC toward the TCP slightly reduced the tolerable range. Placing it directly at the TCP decreased it by less than 10%. Raising the RCC position to 85 mm resulted in failure cases 1) and 2) and reduced the tolerable range to $\approx 80\%$. At 90 mm, instabilities and contact loss led to complete assembly failure. Thus, within realistic bounds, the simplified RCC modeling used here does not significantly impact simulation performance, suggesting that dedicated optimization of the RCC location is not necessary. The primary factors influencing assembly success remain the stiffness of the compliant grippers and the geometric constraints of the connecting pairs.

VI. Conclusion

The main motivation behind the implementation of dynamic simulation is the possibility to omit real-life experiments and utilizing simulation tools as a means to anticipate real-life behavior, as contrasted in Fig. 1. After the preparatory steps in Section IV, the failure cases and tolerable ranges in both simulation and in-situ experiments are evaluated in Section V. A clear dependency of the tolerable range and the stiffness values is only noticeable for the simulated USB assembly task, whereas the tolerable range remains relatively constant for the simulated RJ45 and KET12 task. This behavior was also partly observable in the in-situ experiments, however an offset of the tolerable ranges, as seen in Figs. 9 and 11, and an almost inverse trend as in Fig. 12 have been noted. Especially the slender and long structure of the KET8 assembly task stood out in this work, as strong scattering was noticeable in both simulation and in-situ. As described, this is assumed due to an insufficient modeling of the RCC location, which depends on the infill direction, as this has allowed for a clearer trend analysis as seen in Fig. 7(b). As a main reason for the discrepancy between simulation and real-life scenarios, insufficient modeling and increased complexity of the tasks are determined, leading to falsely simulated contact states during assembly. This has been especially noticeable during the USB assembly task. As seen in Fig 3, the center bar of the USB plug, visualized in Fig. 2(d), is missing, overly simplifying the socket geometry, due to the convex decompositioning process.

Thus, deviations between the CAD models and real-life parts provided by the NIST task board are critical for the sim2real gap. Regarding the real-life setup, minor differences could mitigate the failure type 3) to a failure type 2), especially due to differences in low friction, the initial angle for the established line contact and deviations in the compliance values. While the dependency of tolerable ranges on the stiffness values have indicated deviations, the overall order of magnitude demonstrates similarities. In both simulated and in-situ trials clearly differentiable tolerable ranges are noticeable between the assembly tasks further demonstrating feasibility to simulate the assembly tasks regardless of exact conformity with the real-life values. From the obtained results on the tolerable ranges it is apparent that a universal claim on the optimal design parameters cannot be given. In each task a different parameter combination has achieved the highest tolerable ranges. With an optimized parameter combination an increase by factor ≈ 2.29 was noted, emphasizing the necessity of task-specific optimization, which will be carried out in the proposed future pipeline. The simulation has further shown low sensitivity to minor variations ($\pm 20\%$) of the contact parameters when kept in a realistic range. Regarding the congruence of simulation and real-life validation, the heatmaps in Fig. 8 have indicate a high level of correspondence for the KET assembly tasks, indicating jamming. Again, an increased complexity and overly simplification of the tasks results in higher deviations, which have been noticed for the RJ45 task, as seen in Fig. 8, where an excessive offset has either led to a missed socket, or connector jamming. The limiting factor was determined the geometry and increased complexity of the socket has been identified, as seen in Fig. 2(c). The matching score for the USB assembly task is the lowest over all tasks, as $\approx 27.3\ \%$. Both contact loss and jamming during simulated

IEEE Robotics and Automation Letters (RA-L) paper, presented at ICRA 2026, Vienna, Austria. Cite as RA-L paper.

insertion have been detected, whereas the findings in the real-life experiments where mixed. Either a missed plug, jamming and contact loss have been identified in this case, precluding a clear observable trend. The ambiguous classification of failure cases is attributable to the complications from handling the USB connector as visualized in Fig. 2(d), where the contact established through the form-fit contact from the notch is strongly limited, presumably omitted or falsely approximated in the simulation, which is indicated in Fig. 3. In the real-life scenario this leads to pose uncertainties of the connector in the grasp, introducing instabilities when establishing contact with the socket during the search phase. As described prior, this discrepancy is attributed to the insufficient accuracy of the CAD model of the socket.

In summary, dynamic task simulation has demonstrated feasibility to approximate real-life behavior in regards of the tolerable ranges and observed failure cases, further providing distinguishable tolerable ranges corresponding to the task complexity. However, significant deviations are present, which are attributable to insufficient modeling of the CAD models and are exacerbated by the convex decompositioning process, as well as assumed to the reduced compliance model and the simulation input parameters. It is obvious, that the conformity of the CAD files to the actual counterparts has to be as accurate as possible to reduce the sim2real gap. Complex structures as the connectors and sockets of the RJ45 and USB have been especially sensitive to these simplifications as the deviations have shown, whereas a higher level of conformity was observed for simpler geometries as the KET assembly tasks, showing the current limitation of simulation as a tool for manipulation tasks with complex contact geometry. Failure during insertion (jamming) could be modeled with a small sim2real gap, whereas failure during search and in-hand slip demonstrated a higher sim2real gap. Future work will incorporate the dynamic simulation in the proposed design-pipeline to further assess the ability to determine task-level optimized parameter combinations of passive compliant structures.

REFERENCES

[1] R. M. Hartisch and K. Haninger, "High-speed electrical connector assembly by structured compliance in a finray-effect gripper," *IEEE/ASME Trans. Mechatron.*, vol. 29, no. 2, pp. 810–819, Apr. 2024.

[2] R. Li and H. Qiao, "A survey of methods and strategies for high-precision robotic grasping and assembly tasks—Some new trends," *IEEE/ASME Trans. Mechatron.*, vol. 24, no. 6, pp. 2718–2732, Dec. 2019.

[3] N. Ciblak and H. Lipkin, "Design and analysis of remote center of compliance structures," *J. Robotic Syst.*, vol. 20, no. 8, pp. 415–427, 2003.

[4] S.-K. Yun, "Compliant manipulation for peg-in-hole: Is passive compliance a key to learn contact motion?," in *Proc. IEEE Int. Conf. Robot. Automat.*, 2008, pp. 1647–1652.

[5] C. W. Herron et al., "PANDORA: The open-source, structurally elastic humanoid robot," in *Proc. IEEE-RAS 23rd Int. Conf. Humanoid Robots*, 2024, pp. 24–31.

[6] A. Albu-Schaffer et al., "Soft robotics," *IEEE Robot. Autom. Mag.*, vol. 15, no. 3, pp. 20–30, Sep. 2008.

[7] U. Kim et al., "Displacement sensor integrated into a remote center compliance device for a robotic assembly," *IEEE Access*, vol. 9, pp. 43192–43201, 2021.

[8] J. Shintake, V. Cacucciolo, D. Floreano, and H. Shea, "Soft robotic grippers," *Adv. Mater.*, vol. 30, no. 29, 2018, Art. no. 1707035.

[9] U. Bhagat et al., "Design and analysis of a novel flexure-based 3-DOF mechanism," *Mechanism Mach. Theory*, vol. 74, pp. 173–187, 2014.

[10] R. M. Hartisch and K. Haninger, "Flexure-based environmental compliance for high-speed robotic contact tasks," in *Proc. IEEE/ASME Int. Conf. Adv. Intell. Mechatron.*, 2022, pp. 1608–1613.

[11] K. Haninger, M. Radke, R. Hartisch, and J. Krüger, "Contact information flow and design of compliance," in *Proc. IEEE/ASME Int. Conf. Adv. Intell. Mechatron.*, 2022, pp. 1601–1607.

[12] H.-J. Su, D. V. Dorozhkin, and J. M. Vance, "A screw theory approach for the conceptual design of flexible joints for compliant mechanisms," *J. Mechanisms Robot.*, vol. 1, no. 4, pp. 1–8, 2009.

[13] M. H. Ang and G. B. Andeen, "Specifying and achieving passive compliance based on manipulator structure," *IEEE Trans. Robot. Autom.*, vol. 11, no. 4, pp. 504–515, Aug. 1995.

[14] C. J. Kim, Y.-M. Moon, and S. Kota, "A building block approach to the conceptual synthesis of compliant mechanisms utilizing compliance and stiffness ellipsoids," *J. Mech. Des.*, vol. 130, no. 2, 2008, Art. no. 022308.

[15] L. R. Alacoque, A. Bhattacharyya, and K. A. James, "Compliant mechanism synthesis using nonlinear elastic topology optimization with variable boundary conditions," *Int. J. Numer. Methods Eng.*, vol. 126, no. 1, 2025, Art. no. e7613.

[16] V. Acary, M. Brémond, and O. Huber, "On solving contact problems with coulomb friction: Formulations and numerical comparisons," in *Advanced Topics in Nonsmooth Dynamics: Transactions of the European Network for Nonsmooth Dynamics*. Berlin, Germany: Springer, 2018, pp. 375–457.

[17] F. Hagelskjær, A. Kramberger, A. Wolniakowski, T. R. Savarimuthu, and N. Krüger, "Combined optimization of gripper finger design and pose estimation processes for advanced industrial assembly," in *Proc. 2019 IEEE/RSJ Int. Conf. Intell. Robots Syst.*, 2019, pp. 2022–2029.

[18] Q. Zhang, Z. Hu, W. Wan, and K. Harada, "Compliant peg-in-hole assembly using a very soft wrist," *IEEE Robot. Autom. Lett.*, vol. 9, no. 1, pp. 17–24, Jan. 2024.

[19] Y. Hao et al., "Universal soft pneumatic robotic gripper with variable effective length," in *Proc. 35th Chin. Control Conf.*, 2016, pp. 6109–6114. [Online]. Available: https://ieeexplore.ieee.org/abstract/document/7554316

[20] S. Liu, F. Wang, Z. Liu, W. Zhang, Y. Tian, and D. Zhang, "A two-finger soft-robotic gripper with enveloping and pinching grasping modes," *IEEE/ASME Trans. Mechatron.*, vol. 26, no. 1, pp. 146–155, Feb. 2021.

[21] W. Park, S. Seo, and J. Bae, "A hybrid gripper with soft material and rigid structures," *IEEE Robot. Autom. Lett.*, vol. 4, no. 1, pp. 65–72, Jan. 2019.

[22] W. Crooks, G. Vukasin, M. O'Sullivan, W. Messner, and C. Rogers, "Fin Ray effect inspired soft robotic gripper: From the RoboSoft grand challenge toward optimization," *Front. Robot. AI*, vol. 3, pp. 70–79, 2016.

[23] K. Elgeneidy, P. Lightbody, S. Pearson, and G. Neumann, "Characterising 3D-printed soft fin ray robotic fingers with layer jamming capability for delicate grasping," in *Proc. 2nd IEEE Int. Conf. Soft Robot.*, 2019, pp. 143–148.

[24] X. Wei, M. Liu, Z. Ling, and H. Su, "Approximate convex decomposition for 3D meshes with collision-aware concavity and tree search," *ACM Trans. Graph.*, vol. 41, no. 4, pp. 1–18, 2022.